

Double Crosslinked Hydrogel Dressings based on Triblock Copolymers bearing Anti-Freezing, Anti-Drying and Inherent Antibacterial properties

Qian Wang^a, Xi Liang^b, Lingyi Shen^b, Hong Xu^b, Carl Redshaw,^c Qilong Zhang^{b,*}

^a Translational Medicine Research Center, Guizhou Medical University, Guiyang 550025, P. R. China

^b School of Basic Medical Sciences, Guizhou Medical University, Guiyang 550025, P. R. China

^c Chemistry, School of Natural Sciences, University of Hull, Hull, HU6 7RX, U.K.

* Corresponding author.

E-mail address: sciqlzhang@gmc.edu.cn (Q.-L. Zhang)

Abstract

Bacterial infections typically invade the living tissue of wounds, thereby aggravating the inflammatory response, delaying wound healing or causing further complications. In this paper, *N*-isopropylacrylamide (NIPAM), 1-butyl-3-vinylimidazolium bromide (VBIMBr) and 3-acrylamidophenylboronic acid (AAPBA) were utilized as monomers to afford anti-freezing and anti-drying polymers via free radical polymerization. The antibacterial hydrogel (PNVBA) with inherent antibacterial properties was prepared by crosslinking polymers, and glycerol was introduced to improve the hydrogel anti-freezing and anti-drying properties. PNVBA hydrogels exhibited a water content of 52~65% and swelling ratio of about 4000%, showing a high adsorption capacity of 280 mg·g⁻¹ for bovine serum albumin (BSA). These properties provide an environment conducive to wound repair. Meanwhile, the PNVBA-2 hydrogel exhibits high fracture stress (33.8 kPa) and elongation at break (774%) and can adhere to the surface of different materials through ion-dipole or hydrogen bonding interactions. This allows the hydrogel to adapt to complex dynamic environments when adhering to the wound. Furthermore, the PNVBA hydrogels exhibited high viscoelasticity and good adhesion after freezing at -20 °C or heating at 70 °C for 24 h, with a sterilizing rate of up to 98% against MDR *E. coli* and MRSA. Moreover, a survival rate up to 90% after incubation with L929 cells over 24 h was observed. Therefore, this inherent antibacterial hydrogel with anti-freezing and anti-drying properties

can be used as an excellent alternative material for wound dressings. The work herein provides a new strategy for preparing wound dressings under special environments.

TOC

Keywords: interpenetrating networks, inherent antibacterial activity, anti-freezing, anti-drying, hydrogel dressings

1. Introduction

The skin is the body's first barrier to the external environment, helping to prevent mechanical damage and protects the body's vital organs from invasion and external stimuli, such as ultraviolet light, pathogens and chemical toxins [1,2]. However, the skin is susceptible to multiple types of damage in daily life, as well as diseases, and trauma, including wounds, burns, and bacterial infections [3,4]. When the skin structure is damaged, its function must be restored as soon as possible to ensure the homeostasis of the organism, because the damaged and exposed skin loses its barrier function and is susceptible to bacterial infection [5]. When bacteria compete with the immune system, they invade living tissues, leading to impaired wound healing and amputation. Indeed, millions of people die each year from bacterial infections [6,7]. Moreover, substances such as proteins, cells and necrotic tissues will be produced in the surrounding tissues at the initial stage of wound formation, which will increase the possibility of wound complications and bacterial infection [8]. The wound healing process involves a complex cascade of reactions from many cell types, including hemostasis, inflammation, proliferation and remodeling [9]. Therefore, the wound healing process requires antimicrobials to protect the wound from microbial infection [10]. However, multidrug-resistant bacteria caused by the abuse of antibiotics have become the main culprit of serious pathogenic infections in recent years [11].

At present, a variety of traditional dressings have been applied in clinical treatment, such as bandage, sponge, gauze, fibrin glue and other [12]. However, existing traditional dressings have disadvantages such as poor compatibility, a lack of antibacterial properties, low water content and are unsuitable for loading bioactive materials. Given all these issues, they cannot provide a favorable environment to promote wound healing [13]. Based on this, wound dressings with antibacterial properties have been extensively studied to support skin wound healing and tissue regeneration [14]. In the past, antibacterial polymers were often used as raw materials, and antibacterial agents were added to

dressings to effectively accelerate the healing of infected wounds [15]. However, there are relatively few antibacterial natural polymer materials with good biocompatibility. Additionally, the leaching of antibacterial agents not only weakens the antibacterial activity of the dressing, but also poses potential biosafety risks [16].

Hydrogels are considered to be amongst the most ideal dressing materials and are widely used in biomedical fields due to their high-water content, porous structure and similarity to natural extracellular matrices [17-19]. Yu *et al.* [20] introduced tannic acid/fermionic chelates into dynamically cross-linked chitosan-based hydrogels, which endowed the hydrogels with antibacterial activity allowing them to effectively inhibit Gram-negative and positive bacteria. Li *et al.* [21] designed a composite hydrogel (MPH) with both antibacterial and antioxidant functions based on the copolymerization of *N*-isopropylacrylamide, acrylamide and acryloyl Pluronic 127 (PF127-DA), and the functionalization of a molybdenum disulfide-polydopamine nanozyme (MP). The dual functions of antibacterial and antioxidant activity can effectively improve the wound microenvironment and promote wound healing. Nevertheless, the above hydrogels loaded with antimicrobials have a short antibacterial cycle, which inevitably leads to toxicity and resistance. Furthermore, ordinary hydrogels will freeze and harden at low temperatures (below 0 °C), and they will dry and become brittle at high temperatures (above 50 °C), resulting in failure [22,23].

In this study, a novel inherent antibacterial hydrogel with high swelling ratio, good adsorption capacity, as well as excellent mechanical, anti-freezing and anti-drying properties, was prepared by a two-step method. To avoid the generation of drug-resistant bacteria and to resolve the stability of hydrogel dressings in extreme environments, herein *N*-isopropylacrylamide, 1-butyl-3-vinylimidazolium bromide and 3-acrylamidophenylboronic acid were employed as monomers in free radical polymerization. The hydrogels (PNVBA) with inherent antibacterial properties were prepared after cross-linking, and the anti-freezing and anti-drying properties of the hydrogel were improved by an immersion method. The chemical structure, micromorphology, swelling behavior, mechanical properties, and the anti-freezing/anti-drying properties of the PNVBA hydrogel were systematically studied. The blood compatibility, antibacterial activity and biocompatibility *in vitro* of the PNVBA hydrogel were also analyzed. Moreover, the method reported here provides a new strategy for preparing wound dressings with stabilizing effects for use in special environments.

2. Experimental section

2.1 Materials

N-Isopropylacrylamide (NIPAM, 99%) was purified by recrystallization in hexane and purchased from Sigma-Aldrich (Shanghai) Trading Co., Ltd. Ammonium persulfate (ABS, AR, $\geq 98\%$) and *N,N,N',N'*-tetramethylethylenediamine (TEMED, GC, 99%) were purchased from Shanghai Bio-Chem Technology Co., Ltd. 1-Butyl-3-vinylimidazolium bromide (VBIMBr, 99%), 3-acrylamidophenylboronic acid (AAPBA, 98%) and *N,N*-methylenebisacrylamide (MBA, 99%) were purchased from Beijing innoChem Science & Technology Co., Ltd. Bovine serum albumin (BSA, 98%) was purchased from Shanghai Keya Biotechnology Co., Ltd. Medical alcohol (75%) and normal saline (NS, 0.9%) were purchased from Guizhou Xinyuan Biotechnology Co., Ltd. Strains of multidrug-resistant *Escherichia coli* (MDR *E. coli*) and methicillin-resistant *Staphylococcus aureus* (MRSA) were obtained from the clinical extraction of Affiliated Hospital of Guizhou Medical University. The mouse fibroblasts cell (L929) was purchased from Beyotime Institute of Biotechnology (Shanghai, China). DMEM basic (1X, 8123471) was purchased from Thermo Scientific Co., Ltd. Cell counting kit-8 (CCK-8, MA0218-2-Nov-05H1) was purchased from Dalian Boglin Biotechnology Co., Ltd. Fetal bovine serum (23010701) and Trypsin solutions (0.25%, WH1023C201) were purchased from Procell Life Science & Technology Co., Ltd. Calcein acetoxymethyl ester/propidium iodide (Calcerin-AM/PI, 20230414) staining was purchased from Beijing Solaibao Technology Co., Ltd. Distilled water was prepared in the laboratory (Youpu).

2.2. Preparation of PNVBA hydrogels

1.0 g NIPAM, 1.1 g VBIMBr and a certain amount of AAPBA (how much?) were dissolved in 2 mL deionized water at room temperature. After the above substances were completely dissolved, 0.016 g of the initiator ABS was added with magnetic stirring and stirring was continued for 5 min. Afterwards, 0.008 g of crosslinker MBA was added, after dissolution, it was transferred to a 70 °C water bath for 30 min. with magnetic stirring. After initiation, the reactant was cooled to room temperature and the polymerization accelerator TEMED (30 μ L) was added. After stirring, the system was removed and cured at 70 °C for glue formation. The prepared hydrogel was repeatedly washed with deionized water to remove the unreacted monomers/reagents and was immersed in a mixture of glycerol and water (glycerol: water = 11:2) for 24 h. Following this, the hydrogel was removed and washed with deionized water to remove excess glycerol loaded on the surface. The prepared hydrogels were named PNVBA-0, PNVBA-1, PNVBA-2, PNVBA-3 and PNVBA-4 according to the content of AAPBA, at this time the

AAPBA was 0, 0.5, 1, 1.5 and 2 mg, respectively.

2.3. Physicochemical structure characterization

The chemical structure of the PNVBA hydrogel before and after its synthesis was analyzed using Fourier transform infrared (FT-IR) spectroscopy (Thermo Nicolet iS50). The powdered samples were tested as KBr tablets, and the hydrogel samples were lyophilized and tested using the scanning (ATR) mode with a wavenumber range of 400 to 4000 cm^{-1} . The polymerized PNVBA was analyzed using solid state ^{13}C NMR spectra obtained on a 400 MHz NMR spectrometer (Bruker AVANCE NEO) with a resonance frequency of 100.66 MHz and a spin rate of 8 KHz. The micromorphology of the hydrogel was observed by scanning electron microscope (SEM, HITACHI S-3400N); the samples were broken with liquid nitrogen after lyophilization and tested after gold injection.

2.4. Rheological measurements

The rheological properties of the hydrogel samples were analyzed using a rotary rheometer (Austria-Anton Paar MCR 302). The modulus of the hydrogels was tested using frequency scanning with a strain of 0.5% as the setting parameter; the angular frequency sweep range was 0.1 to 100 $\text{rad}\cdot\text{s}^{-1}$ at ambient temperature, and at a distance of 1 mm.

2.5. Mechanical properties

The mechanical properties of the hydrogel samples were tested by the electronic tensile universal testing machine (TSE-104B). The hydrogel was prepared as a rectangular spline with a length, width and height of 60 mm \times 15 mm \times 2 mm, respectively, and the tensile speed was 50 $\text{mm}\cdot\text{min}^{-1}$ according to GB13022-91. The tensile strength of the hydrogel was calculated from the stress-strain curves.

2.6. Water content and swelling properties

A certain amount of PNVBA hydrogel was weighed and swelled with deionized water, during which the water was changed periodically to replace the glycerol in the gel; the water content of the hydrogel was determined after freeze-drying. The water content (M) was calculated as follows:

$$M(\%) = \frac{(W_o - W_e)}{W_o} \times 100\%$$

The swelling behavior of the PNVBA hydrogels was further analyzed. A circular hydrogel sample of diameter 10 mm and thickness 2 mm was weighed and placed in a 25 $^{\circ}\text{C}$ water bath for swelling. During the swelling, the hydrogel was removed regularly, and the residual water on the surface was removed with filter paper and weighed until the weight was unchanged. The swelling rate (SR) was

calculated as follows [24]:

$$SR (\%) = \frac{(W_t - W_o)}{W_o} \times 100\%$$

Where W_o (g) is the initial weight of the hydrogel, W_e (g) is the weight of the hydrogel after lyophilization, and W_t (g) is the weight of the hydrogel at the swelling time t (h).

2.7. Protein adsorption experiments

Hydrogel pieces weighing about 30 mg were soaked in 75% in ethanol for 1 h, then washed in phosphate buffer (PBS) for 2 h and this was repeated three times to remove ethanol. The adsorption amount of BSA was calculated by incubating the hydrogel with 1 mL BSA ($10 \text{ mg} \cdot \text{mL}^{-1}$) at 37°C for 24 h, and testing the absorbance of BSA at a wavelength of 280 nm using a UV spectrophotometer. Standard curves for BSA were determined at the same wavelength. The calculation formula of BSA adsorption capacity was as follows:

$$\text{Adsorbed BSA (mg} \cdot \text{g}^{-1}) = \frac{C_o - C_e}{W} V$$

where C_o and C_e represent the concentration of BSA before and after adsorption ($\text{mg} \cdot \text{mL}^{-1}$) respectively, W is the initial weight of hydrogel (g), and V is the initial volume of BSA solution (mL).

2.8. Blood compatibility experiments

The blood compatibility of the hydrogel was analyzed by using anticoagulant whole blood of mice (purchased from Guizhou Medical University Animal Center). Anticoagulant whole blood was centrifuged, and 0.5 mL red blood cells were precipitated. 1.0 mL normal saline was added to the mixture and centrifuged. After removing the supernatant, 0.5 mL normal saline was added to dilute the red blood cells. 20 mg of hydrogel was placed in a centrifuge tube with 1 mL of normal saline and 20 μL of red cell suspension and incubated for 4 h at 37°C . Centrifugation was performed after the incubation, and the absorbance of the supernatant at 545 nm was measured using a microplate reader, and the hemolysis ratio of the hydrogel was calculated. Red blood cell suspension/normal saline without water gel was used as negative control, and red blood cell suspension/triple vapor water was used as positive control.

$$\text{Hemolysis ration } (\%) = \frac{D_t - D_{nc}}{D_{pc} - D_{nc}} \times 100\%$$

Specifically, D_t is the absorbance of supernatant after incubation with hydrogel, D_{nc} is the absorbance of

the negative control group without hydrogel, and D_{pc} is positive control group without hydrogel.

2.9. Adhesive performance tests

The tissue adhesive strength of the hydrogels was evaluated by its adhesion to the surfaces of different objects and by using lap-shear tests. In the experiment, different materials were selected for surface adhesion, and the adhesion of the hydrogel on the surface of different materials was recorded by photography. The adhesive strength between the hydrophobic plastic (PP/PE) surface and the PNVBA hydrogel was measured by uniaxial stretching using the lap-shear test (ASTMF2255). The hydrogel was adhered to the middle of two plastic splines, covering an area of 20×10 mm, and then the uniaxial tensile test was carried out using an electronic tensile universal testing machine (TSE-104B) to measure the adhesion strength of the hydrogel at a tensile velocity of $50 \text{ mm} \cdot \text{min}^{-1}$.

2.10. *In vitro* antimicrobial activity

MDR *E. coli* and MRSA were obtained from clinical samples, and the antibacterial effect of hydrogel was measured by the plate method. The hydrogel samples were then alternately immersed in water and 75% ethanol for 30 min and sterilized by ultraviolet light for 30 min. A bacterial suspension of $200 \mu\text{L}$ ($10^7 \text{ CFU} \cdot \text{mL}^{-1}$) and the sterilized hydrogel sample of about $3 \times 3 \times 3$ mm were placed in a 96-well plate, and co-cultured at $37 \text{ }^\circ\text{C}$ for 2 h. After that, the culture solution was diluted to $10^4 \text{ CFU} \cdot \text{mL}^{-1}$ and coated with $100 \mu\text{L}$ on the solid medium. The bacterial colonies on the plates were recorded after incubation at $37 \text{ }^\circ\text{C}$ for 16 h. A bacterial suspension without a hydrogel was used as a control.

The morphology of the bacteria before and after co-incubation with hydrogel was visualized by scanning electron microscopy (JSM-IT700HR). After the sterilized hydrogel was co-cultured with the bacteria, the bacterial precipitates were collected by centrifugation, and the bacteria were blown and suspended by adding the electron microscope fixing solution and fixed at room temperature for 2 h. The bacterial samples were washed with deionized water and fixed with 1% osmic acid. After washing with deionized water, the samples were then dehydrated successively with 30, 50, 70, 80, 90, 95 and 100% (this concentration was repeated three times) ethanol solutions, respectively, with each step performed for about 15 min. Then the samples were lyophilized and the morphology of bacteria was observed. A bacterial suspension without a hydrogel was used as a control.

2.11. Cytotoxicity

The biocompatibility of the hydrogels was analyzed by evaluating the effect of hydrogels on the viability of mouse fibroblasts (L929). 0.05g of sterilized hydrogel was soaked in 10 mL Eagle medium

(DMEM) and incubated in a carbon dioxide (CO₂) incubator for 24 h. After incubation, the medium was filtered to remove the residual hydrogel and stored in a refrigerator at 4 °C for future use. L929 cells were inoculated in a 96-well plate with a density of 10,000 cells/pores and incubated overnight, after which the cells were transferred to a hydrogel extract (100 µL) and cultured in the CO₂ incubator for 24 h and 48 h. Following this, 10 µL CCK-8 reagent was added to the 96-well plate for a further 2 h, and the absorbance of the cell liquid at 450 nm was measured using a microplate reader (BioTek Epoch), and the cell activity was analyzed.

To observe the proliferation of cells, L929 cells were inoculated in a 24-well plate with 10000 cells/pores, after which they were transferred to the hydrogel extract and incubated in a CO₂ incubator for 24 and 48 h. After incubation, the cells were washed twice with PBS and incubated with 1 µL calcein-AM/PI staining solution for 20 min, and the stained cells were observed under fluorescence microscope.

2.12. Statistical analysis

Data analysis was performed using the SPSS 22.0 software. Data related to the mechanical properties, BSA adsorption capacity, blood compatibility, adhesion strength, and bacteria and cell viability of the hydrogel were expressed by the mean and variance, and the final results were determined by three parallel experiments.

3. Results and discussion

3.1. Structural and morphological characterization of PNVBA hydrogels

To obtain inherent antibacterial activity, the hydrogel used NIPAM and VBIMBr as copolymers, and different amounts of AAPBA monomers were introduced to participate in copolymerization to regulate the antibacterial activity and mechanical properties of the hydrogel. After that, the anti-freezing and anti-drying of the PNVBA hydrogels were improved by simple immersion, so that the prepared hydrogel had a broad-spectrum antibacterial activity, good mechanical properties, adhesion, etc. (Figure 1a). The composition of the PNVBA hydrogels was analyzed by FTIR spectroscopy (Figure 1b). Before and after the addition of AAPBA, there are characteristic absorption peaks of methylene (-CH₂, 2940-2878 cm⁻¹), methyl (-CH₃, 2978 cm⁻¹) and isopropyl (1458 and 1381 cm⁻¹) in both PNVBA-0 and PNVBA-1, which are assigned to the aliphatic C-H structural feature of NIPAM and IL [25]. The broad band peak of PNVBA-0 and PNVBA-1 at 3390-3270 cm⁻¹ are the stretching vibrations of O-H and N-H [26], and the stretching vibration peak of imidazole ring skeleton at 1562 cm⁻¹ in VBIMBr appears at

1550 cm^{-1} in the PNVBA-0 and PNVBA-1 infrared spectra and overlap with the bending vibration of the N-H (amide II). The vinyl absorption peaks of NIPAM, VBIMBr and AAPBA at 3140-3070 cm^{-1} and 1655-1615 cm^{-1} were significantly weakened and even disappeared in the PNVBA hydrogels [27], indicating that copolymerization occurs when the double bonds of the three monomers were opened. The stretching vibration absorption peaks at 1578-1648 cm^{-1} are due to the benzene ring in AAPBA, and the stretching vibration peak of B-O bond in AAPBA appears at 1265 cm^{-1} . It is worth noting that the strength of the peak at 1250 cm^{-1} increases with the addition of AAPBA, which is caused by the formation of the BOB bond, indicating that the hydrogel is bonded by covalent bonds. Furthermore, the PNVBA hydrogel exhibited a C=O stretching vibration absorption peak at 1640 cm^{-1} [7]. The chemical structure of the PNVBA hydrogel was verified by ^{13}C NMR spectroscopy (Figure 1c). The resonance signals assigned to VBIMBr were 13.96 (1), 19.97 (2), 32.79 (3), 121.84 (5), 125.00 (6), and 136.34 (4) ppm respectively, for VBIMBr were 22.74 (1'), 50.25 (7), and 174.70 (8) ppm respectively, and for AAPBA were 137.42 (9) and 174.70 (8) ppm respectively. The characteristic resonance signals of the backbone carbon chains after copolymerization of VBIMBr, NIPAM, and AAPBA appeared at 32.79 (b), 41.77 (c), and 58.63 (a) ppm, respectively [28]. According to the results of the ^{13}C NMR spectroscopy, the carbon signals at 126~130 ppm in the carbon-carbon double bond disappeared, indicating that the three monomers were successfully copolymerized and combined into the network, which was consistent with the results of FTIR spectroscopy. In conclusion, PNVBA hydrogels were obtained by the copolymerization of NIPAM, VBIMBr and AAPBA monomers.

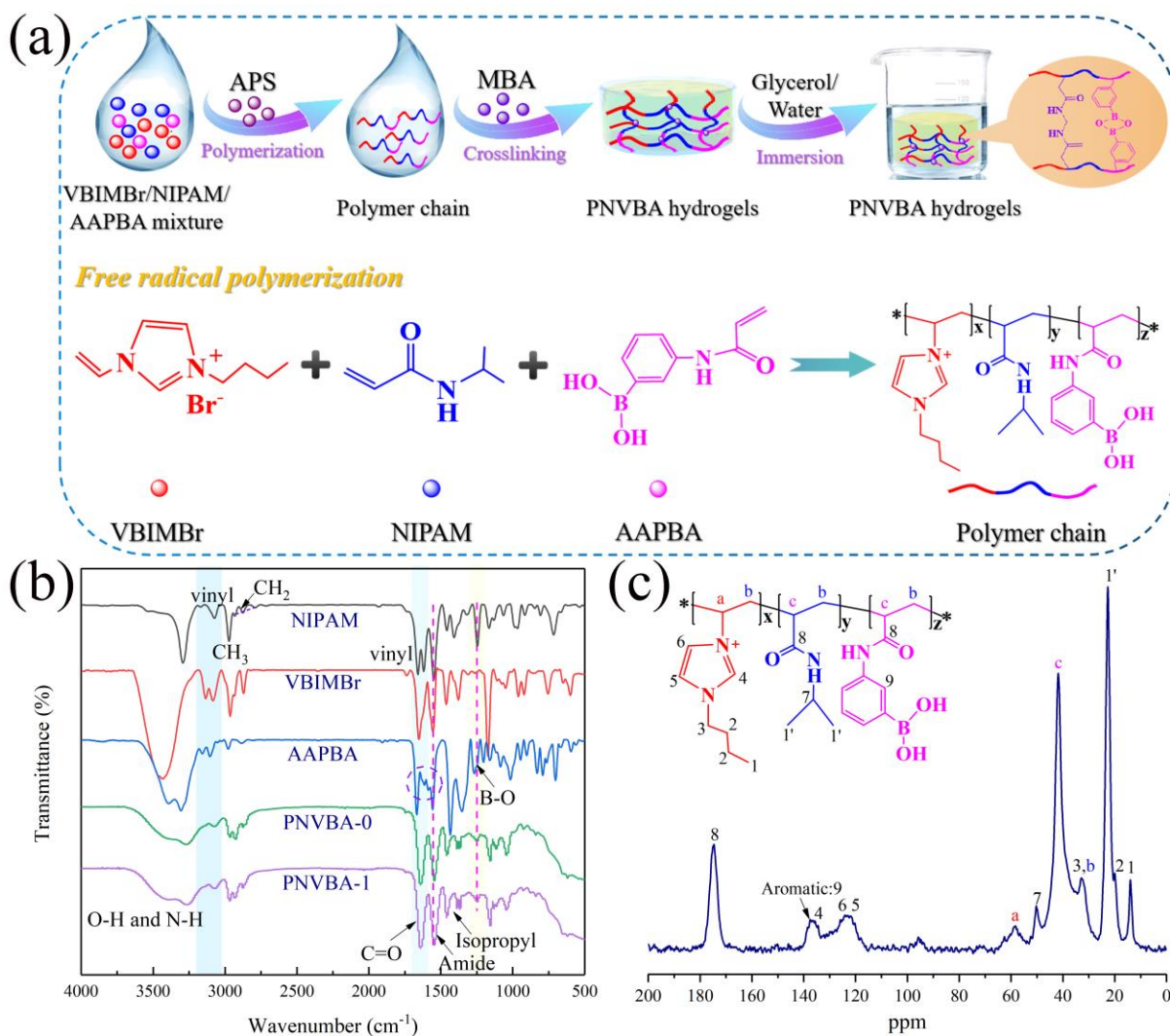


Figure 1. Design and synthesis mechanism of (a) the PNVBA hydrogel; (b) FTIR spectra; (c) ¹³C NMR spectrum.

The microstructure of the PNVBA hydrogels was visualized by scanning electron microscopy (SEM). Due to the anti-freezing and anti-drying properties of the PNVBA hydrogels, all gel samples are difficult to freeze-dry and dry at high temperature directly, so pretreatment is necessary to characterize their microstructure. The hydrogel was first expanded in deionized water for 24h, then soaked in PBS for 24h, rapidly frozen with liquid nitrogen to maintain its structure, and the internal structure was observed after freeze-drying. The PNVBA hydrogels all exhibited an interconnected spongy three-dimensional porous network structure (Figure 2a-e), and the spongy structure endows the gel with high permeability and swelling ratio [29]. With the increase of AAPBA content, the micro size of the hydrogel samples decreased significantly, indicating that the introduction of AAPBA increased the crosslinking density of the hydrogels. It is worth noting that PNVBA-2 exhibits an interpenetrating

network structure (Figure 2c), which stems from the formation of its double-crosslinked network structure (Figure 2f), and thus can enhance the mechanical properties of the hydrogels. With the increase of AAPBA content, the crosslinking density of PNVBA-3 and PNVBA-4 increased, and the BOB bonds present dominated, resulting in a dense network structure of the gel (Figure 2d,e). The dense network structure is one of the important factors to improve the strength of hydrogels [30]. The spongy structure of PNVBA is positive for the absorption of wound exudates, while the good mechanical properties are important for it as a wound dressing [31].

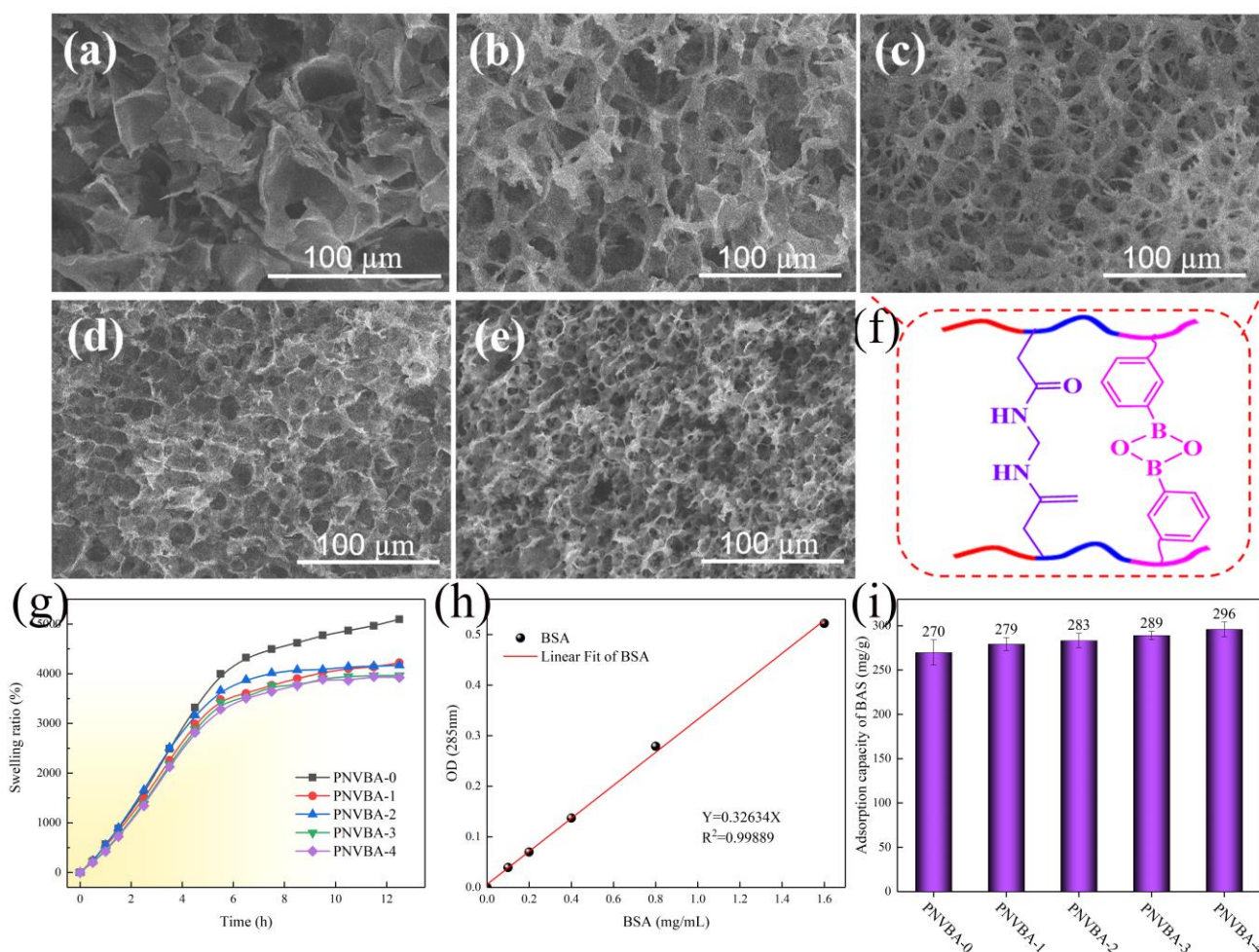


Figure 2. SEM of (a) PNVBA-0; (b) PNVBA-1; (c) PNVBA-2; (d) PNVBA-3; (e) PNVBA-4; (f) double crosslinking diagram; (g) swelling ratio; (h) BSA standard curve; (i) and its adsorption capacity.

3.2. The water content and swelling behavior of the PNVBA hydrogels

Swelling of hydrogels is one of the influencing factors promoting the exchange of cellular metabolites and nutrients [32], and the wet environment provided by hydrogels can effectively promote the hydration of cells, thus promoting wound healing. Therefore, the swelling performance and protein

adsorption capacity of a hydrogel are two important indicators for evaluating a hydrogel as a wound dressing [33]. The water content of hydrogels can be calculated according to the weight difference before and after freeze-drying, and the calculation results of the water content are listed in Table 1. The water content of the PNVBA hydrogels range from 52% and 65%, and the hydrogels with high water content can maintain the wet environment of the wound to promote wound healing. The swelling ratio and morphological changes before and after swelling of the PNVBA hydrogels at room temperature (25 °C) are shown in Figures 2g and S1. All hydrogels showed dynamic swelling patterns with rapid swelling at the beginning, the swelling equilibrium is approached at 8h, and the swelling speed becomes slow (Figure 2g). As the crosslinking bond of the borate group in the hydrogel increased, the swelling ratio of the PNVBA hydrogels at 12h was lower than that of PNVBA-0 without AAPBA. The swelling ratios for PNVBA-0, PNVBA-1, PNVBA-2, PNVBA-3 and PNVBA-4 were 5097%, 4222%, 4170%, 3963% and 3925%, respectively. Notably, the swelling ratio of the hydrogels at 12h does not change significantly with the increase of the AAPBA content, indicating that the content of AAPBA is not the main factor affecting the swelling ratio of the hydrogel, which is related to the formation of reversible boronic-ester bonds. In addition, the volume of the hydrogel increased sharply after swelling, and the color of the hydrogel changed from light yellow to near colorless due to the absorption of a large amount of water (Figure S1). The excellent swelling ratio and protein adsorption capacity of the hydrogels are conducive to wound healing [34], so the protein adsorption capacity of the hydrogels was studied next.

Table 1. Water content of PNVBA hydrogels

Samples	PNVBA-0	PNVBA-1	PNVBA-2	PNVBA-3	PNVBA-4
Original weight/g	0.0936	0.1023	0.0797	0.1158	0.0876
Freeze-dried weight/g	0.0369	0.0441	0.0301	0.0546	0.0364
Water content/%	60.58	56.89	62.23	52.85	58.45

3.3. BSA adsorption capacity of the PNVBA hydrogels

As a wound dressing, hydrogels should also have good protein adsorption capacity, which can timely absorb a large number of protein-like secretions produced by the injured tissues in the initial stage of wound healing, so as to reduce the possibility of bacterial infection of the wound. In the experiment for the PNVBA hydrogel protein adsorption, BSA was used as the model protein, and the

experimental results are shown in Figure 2h,i. The PNVBA hydrogels showed good adsorption capacity for BSA, and with the increase of AAPBA content, the adsorption capacity of the hydrogel to protein gradually increased. The adsorption capacities of PNVBA-0, PNVBA-1, PNVBA-2, PNVBA-3, and PNVBA-4 for BSA were 269.94, 279.42, 283.40, 289.11 and 296.02 mg·g⁻¹, respectively. The high BSA adsorption capacity of the PNVBA hydrogels is derived from the positively charged imidazole ring group in VBIMBr and the amino group in NIPAM can generate electrostatic interaction with negatively charged BSA, so that BSA can be adsorbed on the hydrogel [27]. Meanwhile, the boronic acid group of AAPBA can also produce electrostatic interactions with the negatively charged BSA, thus improving the adsorption capacity of the hydrogel for BSA. The good protein adsorption capacity of PNVBA hydrogels can provide an environment favorable for wound recovery.

3.4. Mechanical properties of the PNVBA hydrogels

The mechanical properties of the PNVBA hydrogels were analyzed by tensile and rheological testing at room temperature. Figure 3 shows the results of the tensile test of the hydrogel. The tensile stress-strain curves of the different hydrogels showed that PNVBA hydrogels have good mechanical properties (Figure 3a) and can be stretched to 5-8 times their original length (Figure 3b, c). The fracture stress of the PNVBA hydrogels increased with the increase of AAPBA content (Figure 3d), and its elongation at breaking point was lower than that of PNVBA-0 except PNVBA-2 (Figure 3c). This indicates that the introduction of AAPBA affords a hydrogel with strong stretching ability, which is due to the boronic acid groups of AAPBA forming a reversible BOB bond in the hydrogel and thereby improving the degree of crosslinking present [35]. It is worth noting that the PNVBA-2 hydrogel with an appropriate amount of AAPBA can improve the fracture stress (33.8 kPa) while maintaining a high elongation at break (774%), which is derived from the formation of its interpenetrating network to enhance the mechanical properties of the hydrogel. With the increase of AAPBA content, PNVBA-3 and PNVBA-4 exhibited dense network structures due to the increased BOB bonds present, resulting in a decrease in elongation at break. Good mechanical properties enable hydrogels to be well adapted to complex dynamic environments when adhering to wound sites [36].

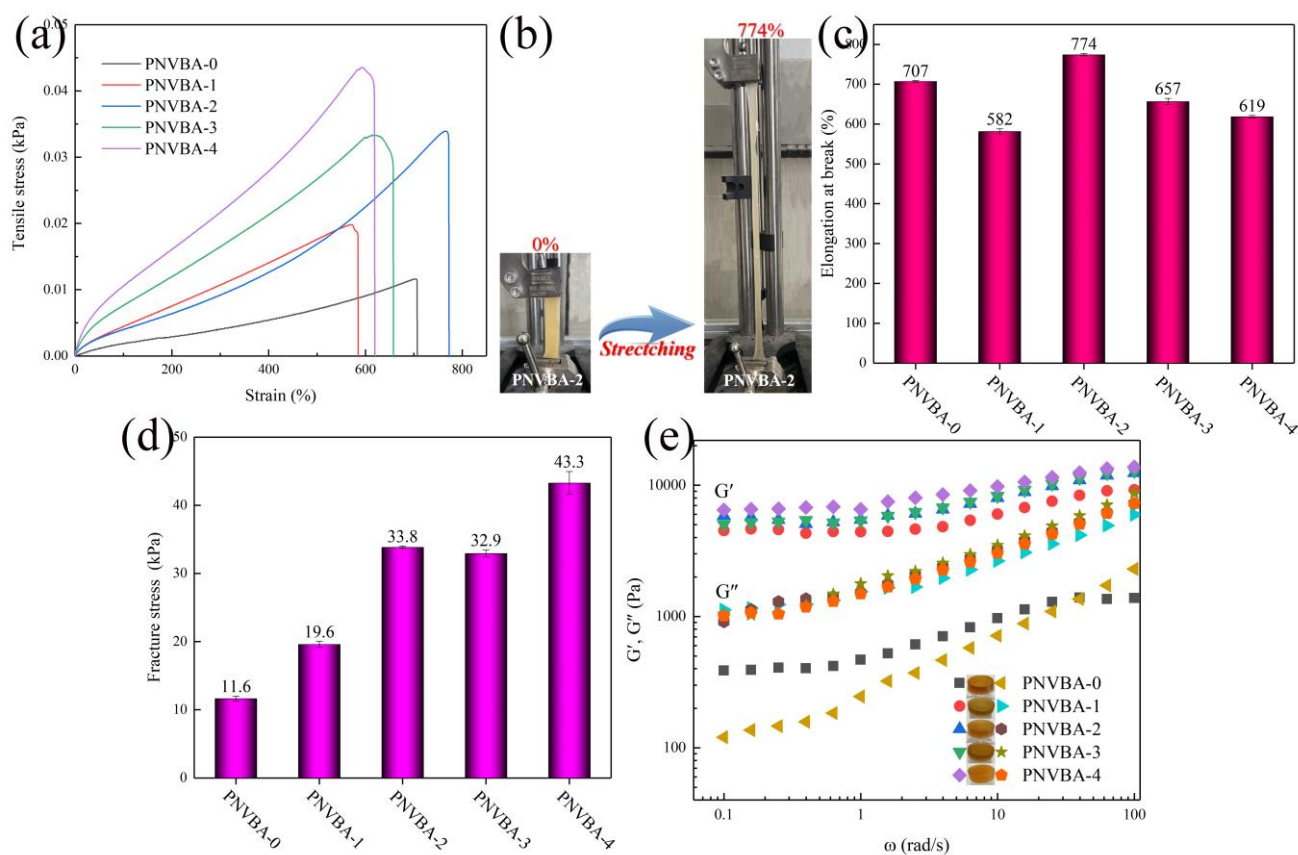


Figure 3. Stress-strain curves (a), tensile photo (b), elongation break (c), fracture stress (d), and rheological results (e) of PNVBA hydrogels.

The rheological results of the PNVBA hydrogels are shown in Figure 3e. At different angular frequencies, the energy storage modulus (G') and loss modulus (G'') of the PNVBA hydrogels showed an increasing trend with the increase of angular frequency. The G' value is always higher than that of G'' , which indicates that the hydrogel forms a crosslinked network structure, and has good strength and toughness, so it is not prone to permanent deformation [37]. The G'/G'' value exceeds 1 in the low frequency range ($0.1-1 \text{ rad}\cdot\text{s}^{-1}$), indicating that the hydrogels undergo elastic deformation and have a solid-like behavior [38]. At high frequency, the G'' value of PNVBA-0 is greater than G' , which is related to its low degree of crosslinking, and the crosslinking network is completely destroyed at high frequency showing mobility. With the introduction of AAPBA, the formation of BOB bonds in the hydrogel increased the degree of crosslinking, making the G' and G'' values of the hydrogel much higher than PNVBA-0. The G' and G'' values of PNVBA-2, PNVBA-3 and PNVBA-4 were similar, implying that the hydrogels exhibited good strength and toughness, which can meet the mechanical requirements of their use as wound dressings.

3.5. Viscosities of the PNVBA hydrogels

The adhesion of hydrogels will affect their practical application as wound dressings, including sealing wounds, hemostasis, tissue adhesion and improving tissue recovery [32]. The adhesion of the PNVBA hydrogels on the different surfaces is shown in Figure 4a. The multiple interactions (covalent and non-covalent) between the functional groups of the PNVBA hydrogels and different material surfaces allow it to stably adhere to materials with different weights (2~18g) [39], including PTEF magnetons, rubber stoppers, glass bottles, PS culture dishes, PP blue caps, pig skins, sticky notes, and iron scissors. The adhesion of the hydrogel was evaluated using lap-shear tests, and a schematic of lap-shear strength measurements is shown in Figure 4b. The prepared hydrogels were adhered between the PP/PE mixed plastic substrate, and the adhesion strength of the hydrogel was measured by tensile shear (Figure 4c). With the increase of AAPBA content, the adhesion strength of PNVBA firstly increases and then decreases. This is due to the functional groups of PNVBA-0 containing charged ions and amino-groups interacting with the charged functional groups or hydrogen bond donors of the materials through ion-dipole or hydrogen bonding interactions, thereby improving the biological adhesion capacity [40]. However, PNVBA-0 has the lowest adhesion strength obtained by tensile shear measurements, resulting from its poor mechanical properties. With the increase of AAPBA content, the mechanical properties of PNVBA-1 and PNVBA-2 are improved, while the charged groups in the hydrogel (such as COO^-) are increased, which enhances the interaction with the material, so its adhesion was improved. The large number of carboxyl groups in PNVBA-3 and PNVBA-4 will not only form BOB bonds, but also consume amino groups and interact with charged ions, so their adhesion was reduced.

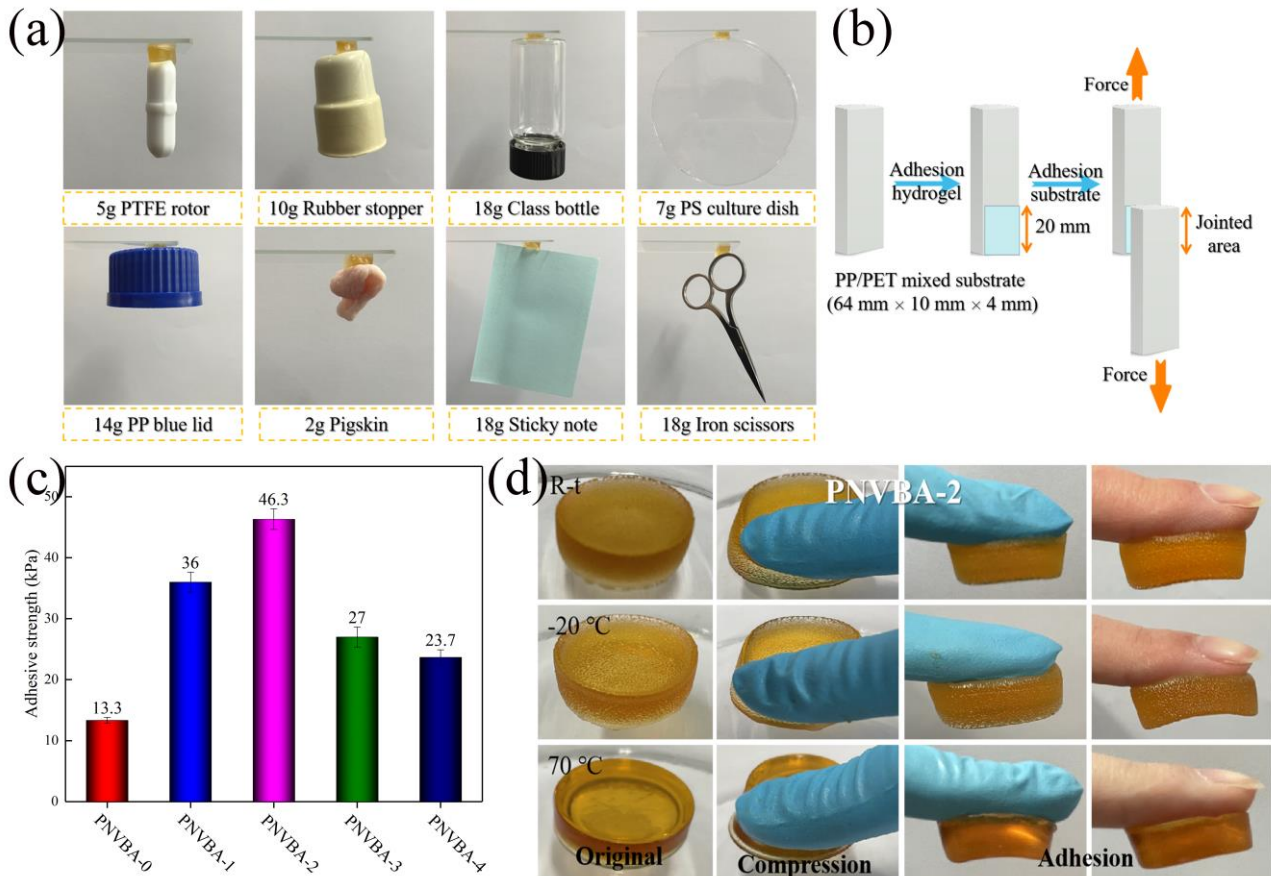


Figure 4. (a) PNVBA hydrogels adhesion to the surface of different materials; (b) schematic representation of lap-shear tests; (c) adhesive strength; (d) photos of anti-freezing/anti-drying experiments.

3.6. Anti-freezing and anti-drying properties of the PNVBA hydrogels

Hydrogels contain a lot of water and are easy to freeze at low temperatures, showing rigidity and are easily broken. They readily lose water at high temperatures, resulting in shrinkage and fragility of the hydrogels, which greatly limits the use of hydrogels in cold or hot environments. The anti-freezing and anti-drying of the PNVBA hydrogels were tested by freezing at $-20\text{ }^{\circ}\text{C}$ and heating at $70\text{ }^{\circ}\text{C}$ for 24 h, respectively. The hydrogel was soaked with glycerol/water mixture to improve the anti-freezing and anti-drying properties. After 24h of freezing or heating, the PNVBA hydrogels still exhibited high viscoelasticity to maintain large deformation and can restore its original state after high compression (Figures 4d and S2). In addition, the frozen or heated hydrogels still showed good adhesion, which was basically the same as the original hydrogels (room temperature $25\text{ }^{\circ}\text{C}$). There are two reasons for the anti-freezing and anti-drying properties of the PNVBA hydrogels: firstly, the positively charged

VBIMBr fragments in the hydrogel inhibit the crystallization of water molecules at low temperature ($-20\text{ }^{\circ}\text{C}$), that is, “free water” cannot form large-scale crystallization after forming small ice crystals; this fragment strongly interacts with highly polar water at high temperature ($70\text{ }^{\circ}\text{C}$) to prevent loss of water molecules [33]. The other is that the hydrogel soaked in glycerol/water mixture loses water molecules at the lower part of the concentration difference, while a small amount of glycerol molecules enter the hydrogel and produce hydrogen bonding with water molecules and gel groups, thus inhibiting the low temperature crystallization and high temperature evaporation of water molecules. The PNVBA hydrogels have anti-freezing, anti-drying and excellent tissue adhesion, conferring the hydrogels with universal soft tissue adhesion [41]. As shown in the video, the frozen or heated hydrogel remained firmly attached to the volunteers’ fingers, becoming deformed by following the movement of the hand joint, and allowing repeated multiple adhesion without damaging the skin (Supplementary Video S1).

3.7. Hemolysis analysis

The cell compatibility and blood compatibility of hydrogels greatly influence their application in the biomedical field [42]. Blood compatibility is one of the evaluation conditions to judge whether hydrogels can be used as medical materials, and its hemolysis ratio reflects the blood compatibility of the hydrogels [43]. A hemolysis ratio higher than 5% indicates that the material will cause hemolysis, which leads to certain damage to the body, so it cannot be used as a medical material. The blood compatibility experimental results for the PNVBA hydrogels are shown in Figure 5a. As a positive control, red blood cells were ruptured due to osmotic pressure in the three steaming water, resulting in a bright red color in the supernatant [44]. Normal saline (NS) maintained the osmotic pressure of the red blood cells, and the supernatant showed colorless and transparent as a negative control. After 4h of co-incubation with the PNVBA hydrogel, its supernatant was similar to the negative control group NS, indicating that the prepared hydrogel had good blood compatibility and was a non-hemolytic material, which could be used as a medical dressing.

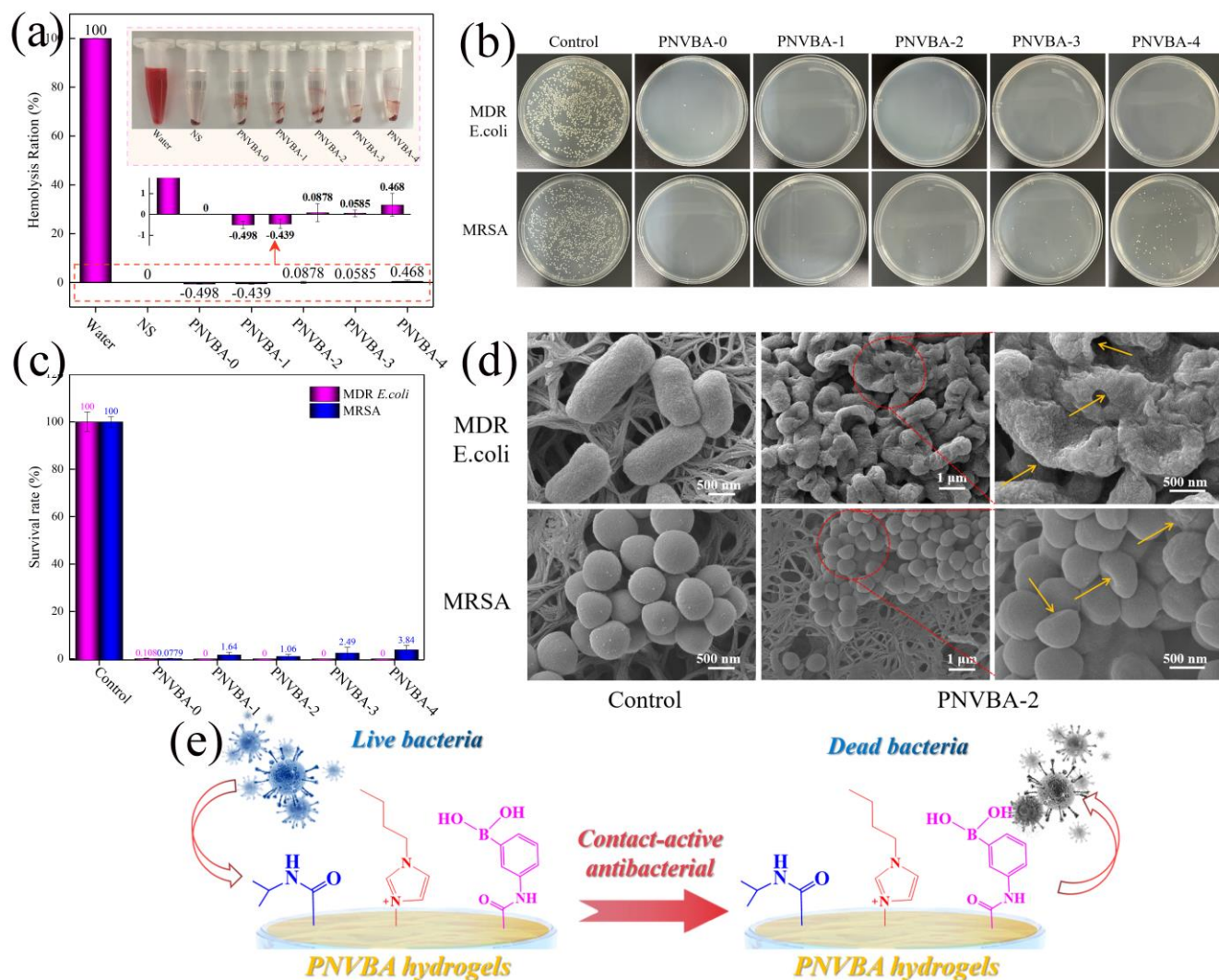


Figure 5. Blood compatibility (a), antibacterial photos (b), bacterial survival rate (c), SEM images before and after treatment (d) and schematic diagram of antibacterial mechanism (e) of PNVBA hydrogels.

3.8. Antibacterial activity evaluation

The antibacterial properties of hydrogels were analyzed by colony counting method, and multidrug-resistant *Escherichia coli* (MDR *E. coli*) and methicillin-resistant *Staphylococcus aureus* (MRSA) were used as the experimental objects. Compared with the control group that was not treated with the hydrogel, the survival rate of MDR *E. coli* and MRSA after hydrogel treatment was significantly reduced, showing good antibacterial activity (Figure 5b,c). Notably, PNVBA-0, PNVBA-1, PNVBA-2, PNVBA-3, and PNVBA-4 showed significant antibacterial activity against MDR *E. coli*, and the number of colonies decreased to zero with the introduction of AAPBA (Figure 5b). This is derived from the fact that AAPBA can promote the interaction between the lipopolysaccharide on the leaflet

outside the cell membrane of Gram-negative bacteria and the boron-polyol to improve the antibacterial activity of hydrogels against Gram-negative bacteria [45]. With the increase of AAPBA content, the antibacterial activity of the hydrogels against MRSA decreased slightly, but the highest survival rate of bacteria was only 3.84% (Figure 5c). The excellent antibacterial properties of the PNVBA hydrogels stem from their positively charged cations, which can attract negatively charged bacteria through electrostatic interactions, and combine with the cell membrane of the bacteria to destroy the integrity of the membrane. This results in the leakage of intracellular material and the inactivation of bacterial enzymes, eventually killing the bacteria [46]. The crosslinking density of the hydrogels increased with the content of AAPBA. Meanwhile, the amino groups were partially consumed when the AAPBA was introduced [47], resulting in a slight increase in the number of MRSA colonies after PNVBA hydrogel treatment. Nevertheless, the antibacterial activity of PNVBA-2 remained above 98%, while it had a good swelling ratio and protein adsorption capacity. Furthermore, the PNVBA hydrogels have inherent antibacterial activity rather than through the release of antibacterial agents, and there was no antibacterial circle on agar plates as shown in Figure S3, indicating that the PNVBA hydrogels do not cause drug-resistance in bacteria.

To analyze the effect of the PNVBA hydrogels on bacteria, the morphological changes of bacteria before and after PNVBA-2 hydrogel treatment were observed by scanning electron microscopy. As shown in Figure 5d, compared to MDR *E. coli* and MRSA with full, smooth rod and spherical shapes as control groups, the hydrogel-treated MDR *E. coli* and MRSA cells were severely wrinkled and ruptured. The wrinkled morphology, the cell wall collapse and perforation of the bacterial cell surface were clearly observed in the enlarged image, allowing the efflux of the cytoplasm and other substances inside the bacterial cell, which leads to bacterial apoptosis. The above results indicate that the PNVBA hydrogels exhibit good inherent antibacterial activity through a contact-active antibacterial mode (Figure 5e), which suggests it has the potential to prevent wound infection when used as a wound dressing, and without toxicity and resistance.

3.9. Biocompatibility analysis

As a biomedical material, the biosafety of the PNVBA hydrogels greatly influences their use as a wound dressing [47]. To evaluate the biocompatibility of the PNVBA hydrogels, mouse fibroblasts (L929 cells) were selected as model objects *in vitro* based on literature studies [37,48]. The cytotoxicity of the hydrogel extracts was determined by the detection method of the CCK-8 kit [49]. Figure 6a,b

shows the cell activity of L929 cells after co-incubation with different PNVBA hydrogel extracts for 24 h and 48 h. The cell survival rate of the PNVBA hydrogel extracts after incubation of L929 cells for 24 h exceeded 90% (except only 88% for PNVBA-0), the cell survival rate of PNVBA-2 and PNVBA-3 approached 100%, and that of PNVBA-4 even exceeded 100%. After 48 h incubation, the cell survival rate of all PNVBA hydrogels was higher than 80% except PNVBA-0, with PNVBA-1, PNVBA-2 and PNVBA-3 was higher than 85%. These results indicated that the PNVBA hydrogels containing AAPBA had no obvious toxicity toward L929 cells.

To further observe the morphology and survival of the cells, calcein acetoxymethyl ester/propidium iodide (Calcein-AM/PI) staining was used to detect the live/dead cells. Calcein-AM can penetrate the live cell membrane to stain the live cells and emit strong green fluorescence. PI can be embedded in the cellular DNA double helix to produce red fluorescence, staining only for dead cells. The live and dead cells were observed simultaneously by activating Calcein-AM and PI at 450 nm. The staining results of live/dead cells after different PNVBA hydrogel extracts were co-incubated with L929 cells for 24 h and 48 h are shown in Figures 6c and S4. After 24 h and 48 h of incubation with different PNVBA hydrogel extracts, the L929 cells still showed a spindle-shaped, and only a very small number of dead cells with red fluorescence were observed. The number of L929 cells increased significantly after 48 h of incubation, which also indicated that the PNVBA hydrogel extract was non-toxic toward L929 cells and can be applied as a wound dressing for wound healing. Furthermore, the NIPAM contained in the matrix component of the PNVBA hydrogel enables the presence of secondary amine structures on the gel surface, which provides a favorable weakly basic microenvironment for cell growth [50,51]. In summary, the PNVBA hydrogels have good biocompatibility for L929 cells and can be used as biomedical materials in wounds.

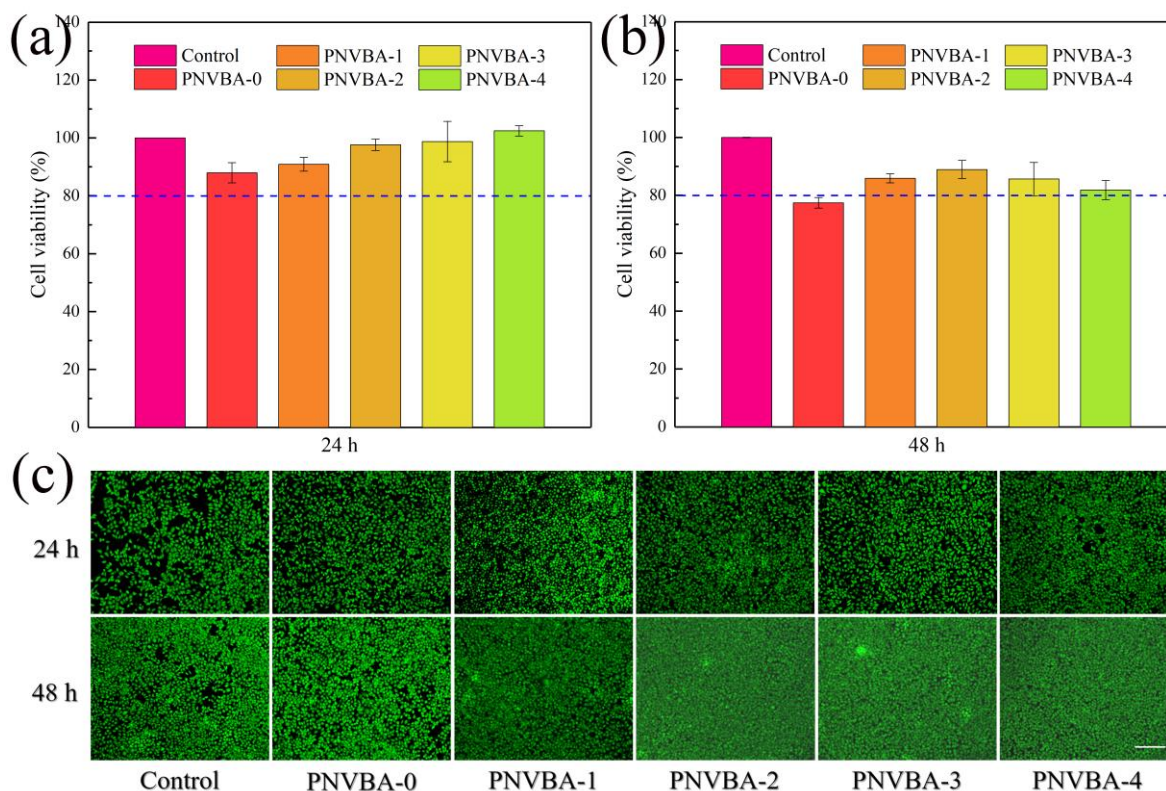


Figure 6. Cell viability after PNVBA hydrogel treatment: (a) 24h; (b) 48h; (c) viable cells staining results.

4. Conclusions

Herein, NIPAM, VBIMBr and AAPBA were designed as monomers to obtain anti-freezing and anti-drying polymers by free radical polymerization, PNVBA hydrogels with inherent antibacterial properties were prepared by crosslinking polymers, and the immersion method was used to improve the anti-freezing and anti-drying of the hydrogel. The PNVBA hydrogel exhibits a high-water content, swelling ratio, and BSA adsorption capacity of $280 \text{ mg}\cdot\text{g}^{-1}$, which can provide an environment conducive to wound repair. The PNVBA-2 hydrogel exhibits a high fracture stress (33.8 kPa) and elongation at break (774%) and can adhere to the surface of different materials through ion-dipole or hydrogen bonding interactions, allowing the hydrogel to adapt to complex dynamic environments when adhering to the wound. Meanwhile, the PNVBA-2 hydrogel showed excellent anti-freezing and anti-drying properties, good blood compatibility, remarkable antibacterial activity and biocompatibility. Therefore, this inherent antibacterial hydrogel with anti-freezing and anti-drying properties can be used as an excellent alternative material for wound dressings and can be used to promote wound healing in skin tissue engineering.

Declaration of Competing Interest

The authors declare that they have no known competing financial interests or personal relationships that could have appeared to influence the work reported in this paper.

Acknowledgments

The authors gratefully acknowledge the National Natural Science Foundation of China [grant number 22065009 and 22066007] and Guizhou Medical University Startup Project of Doctor Scientific Research [grant number YJ2022-BK066]. CR thanks the University of Hull for support.

Appendix A. Supplementary data

Performance analysis figures of hydrogel samples, including the before and after swelling, the anti-freezing and anti-drying, the contact antibacterial activity and the staining results of dead cells.

Appendix B. Supplementary Video S1.

References

- [1] Y. Liang, J. He, B. Guo, Functional hydrogels as wound dressing to enhance wound healing, *ACS Nano*, 2021, 15, 12687-12722.
- [2] L. Norlen, M. Lundborg, C. Wennberg, A. Narangifard, B. Daneshmandi, The skin's barrier: a cryo-EM based overview of its architecture and stepwise formation, *J. Invest. Dermatol.*, 2022, 142(2), 285-292.
- [3] J. Liu, X.S. Xie, T. Wang, H. Chen, Y.H. Fu, X.Y. Cheng, J.B. Wu, G. Li, C.M. Liu, H. Liimatainen, Z.Z. Zheng, X.Q. Wang, D.L. Kaplan, Promotion of wound healing using nanoporous silk fibroin sponges, *ACS Appl. Mater. Interfaces*, 2023, 15(10), 12696-12707.
- [4] R. Portela, C. R. Leal, P. L. Almeida, R. G. Sobral, Bacterial cellulose: a versatile biopolymer for wound dressing applications, *Microbial Biotechnology*, 2019, 12(4), 586-610.
- [5] Y. Zhao, Y. Sun, Y. Zhang, X. Ding, N. Zhao B. Yu, et al. Well-defined gold nanorod/ polymer hybrid coating with inherent antifouling and photothermal bactericidal properties for treating an infected hernia, *ACS Nano*, 2020, 14(2), 2265-2275.
- [6] W.-C. Huang, R. Ying, W. Wang, Y.N. Guo, Y.J. He, X.Y. Mo, C.H. Xue, X.Z. Mao, A macroporous hydrogel dressing with enhanced antibacterial and anti-inflammatory capabilities for accelerated wound healing, *Adv. Funct. Mater.*, 2020, 30(21), 2000644.
- [7] B. Liu, J. Li, Z. Zhang, J. D Roland, B. P Lee, pH responsive antibacterial hydrogel utilizing

catechol-boronate complexation chemistry, *Chemical Engineering Journal*, 2022, 441, 135808.

[8] W. J. Yang, X. Tao, T. Zhao, L. Weng, E.-T. Kang, L. Wang, Antifouling and antibacterial hydrogel coatings with self-healing properties based on a dynamic disulfide exchange reaction, *Polym. Chem.*, 2015, 6, 7027-7035.

[9] Y. L. Xu, H. L. Chen, Y. F. Fang, J. Wu, Hydrogel combined with phototherapy in wound healing, *Adv. Healthc. Mater.*, 2022, 11(16), 2200494.

[10] K. Ito, A. Saito, T. Fujie, K. Nishiwaki, H. Miyazaki, M. Kinoshita, D. Saitoh, S. Ohtsubo, S. Takeoka, Sustainable antimicrobial effect of silver sulfadiazine-loaded nanosheets on infection in a mouse model of partial-thickness burn injury, *Acta Biomater.*, 2015, 24, 87-95.

[11] E. D. Brown, G. D. Wright, Antibacterial drug discovery in the resistance era, *Nature*, 2016, 529, 336-343.

[12] J. Zhou, R. Cha, Z. Wu, C. Zhang, Y. He, H. Zhang, K. Liu, M. S. Fareed, Z. Wang, C. Yang, Y. Zhang, W. Yan, K. Wang, An injectable, natural peptide hydrogel with potent antimicrobial activity and excellent wound healing-promoting effects, *Nano Today*, 2023, 49, 101801.

[13] W. Liu, W. Ou-Yang, C. Zhang, Q. Wang, X. Pan, P. Huang, C. Zhang, Y. Li, D. Kong, W. Wang, Synthetic polymeric antibacterial hydrogel for methicillin-resistant staphylococcus aureus-infected wound healing: nanoantimicrobial self-assembly, drug- and cytokine-free strategy, *ACS Nano*, 2020, 14, 12905-12917.

[14] D. M. Zhang, G. K. Cai, S. Mukherjee, Y. J. Sun, C. H. Wang, B. J. Mai, K. Q. Liu, C. Yang, Y. S. Chen, Persistently moisture-retentive, and wearable biomimetic film inspired by fetal scarless repair for promoting skin wound healing, *ACS Appl. Mater. Interfaces*, 2020, 12(5), 5542-5556.

[15] S. X. Yi, Y. Zhou, J. M. Zhang, M. Wang, S. H. Zheng, X. Yang, L. Duan, R. L. Reis, F. Y. Dai, S. C. Kundu, B. Xiao, Flat silk cocoon-based dressing: daylight-driven rechargeable antibacterial membranes accelerate infected wound healing, *Adv. Healthcare Mater.*, 2022, 11(21), 2201397.

[16] S. C. M. Fernandes, P. Sadocco, A. Aonso-Varona, T. Palomares, A. Eceiza, A. J. D. Silvestre, I. Mondragon, C. S. R. Freire, Bioinspired antimicrobial and biocompatible bacterial cellulose membranes obtained by surface functionalization with aminoalkyl groups, *ACS Appl. Mater. Interfaces*, 2013, 5(8), 3290-3297.

[17] J. Y. Zhao, D. Diaz, D. N. Wu, M. Peng, Y. Y. Wang, J. Q. Zeng, R. Narain, Dual-cross-linked network hydrogels with multiresponsive, self-Healing, and shear strengthening properties,

Biomacromolecules, 2020, 22(2), 800-810.

[18] S. Guo, M. Yao, D. Zhang, Y. He, R. Chang, Y. Ren, F. Guan, One-step synthesis of multifunctional chitosan hydrogel for full-thickness wound closure and healing, *Adv. Healthc. Mater.*, 2021, 11, e2101808.

[19] J. Ouyang, Q. Bu, N. Tao, M. Chen, H. Liu, J. Zhou, J. Liu, B. Deng, N. Kong, X. Zhang, T. Chen, Y. Cao, W. Tao, A facile and general method for synthesis of antibiotic-free protein-based hydrogel: wound dressing for the eradication of drug-resistant bacteria and biofilms, *Bioact. Mater.*, 2022, 18, 446-458.

[20] P. F. Li, W. Q. She, Y. D. Luo, D. F. He, J. L. Chen, N. Ning, Y. L. Yu, S. D. Beer, S. Y. Zhang, One-pot, self-catalyzed synthesis of self-adherent hydrogels for photo-thermal, antimicrobial wound treatment, *J. Mater. Chem. B*, 2021, 9(1), 159-169.

[21] Y. Li, P. Yu, J. Wen, H. Sun, D. Wang, J. Liu, J. Li, H. Chu, Nanozyme-based stretchable hydrogel of low hysteresis with antibacterial and antioxidant dual functions for closely fitting and wound healing in movable parts, *Adv. Funct. Mater.*, 2022, 32(13), 2110720.

[22] Y. Feng, S. Wang, Y. Li, W. Ma, G. Zhang, M. Yang, H. Li, Y. Yang, Y. Long, Entanglement in smart hydrogels: fast response time, anti-freezing and anti-drying, *Adv. Funct. Mater.*, 2023, 33(21), 2211027.

[23] G. Li, J. Chen, Z. Yan, S. Wang, Y. Ke, W. Luo, H. Ma, J. Guan, Y. Long, Physical crosslinked hydrogel-derived smart windows: anti-freezing and fast thermal responsive performance, *Mater. Horiz.*, 2023, 10, 2004-2012.

[24] S. J. Feng, Q. R. Li, S. X. Wang, B. Wang, Y. T. Hou, T. Zhang, Tunable dual temperature-pressure sensing and parameter self-separating based on ionic hydrogel via multisynergistic network design, *ACS Appl. Mater. Interfaces*, 2019, 11(23), 21049-21057.

[25] T. Elshaarani, H. Yu, L. Wang, L. Lin, N. Wang, K. U. R. Naveed, L. Zhang, Y. Han, S. Fahad, Z. Ni, Dextran-crosslinked glucose responsive nanogels with a selfregulated insulin release at physiological conditions, *Eur. Polym. J.*, 2020, 125, 109505-109510.

[26] D. Shen, H. Yu, L. Wang, X. Chen, J. Feng, C. Li, W. Xiong, Q. Zhang, Glucose-responsive hydrogel-based microneedles containing phenylborate ester bonds and N-isopropylacrylamide moieties and their transdermal drug delivery properties, *Eur. Polym. J.*, 2021, 148, 110348.

[27] D. Li, X. Fei, L. Xu, Y. Wang, J. Tian, Y. Li, Pressure-sensitive antibacterial hydrogel dressing for wound monitoring in bed ridden patients, *J. Colloid Interface Sci.*, 2022, 627, 942-955.

- [28] S. Z. M. Rasib, Z. Ahmad, A. Khan, H. M. Akil, M. B. H. Othman, Z. A. A. Hamida, F. Ullah. Synthesis and evaluation on pH- and temperature-responsive chitosan-p(MAA-co-NIPAM) hydrogels, *Int. J. Biol. Macromol.*, 2018, 108, 367-375.
- [29] X. W. Yang, D. K. Debeli, G. R. Shan, P. J. Pan, Selective adsorption and high recovery of La^{3+} using graphene oxide/poly (N-isopropyl acrylamide-maleic acid) cryogel, *Chem. Eng. J.*, 2020, 379, 122335.
- [30] Y. L. Zhang, K. X. Chen, Y. S. Li, J. Lan, B. Yan, L. Y. Shi, R. Ran, High-strength, self-healable, temperature-sensitive, MXene-containing composite hydrogel as a smart compression sensor, *ACS Appl. Mater. Interfaces*, 2019, 11(50), 47350-47357.
- [31] H. Fang, J. Wang, L. Li, L. Xu, Y. Wu, Y. Wang, X. Fei, J. Tian, Y. Li, A novel high-strength poly(ionic liquid)/PVA hydrogel dressing for antibacterial applications, *Chem. Eng. J.*, 2019, 365, 153-164.
- [32] D. K. Patel, K. Ganguly, J. Hexiu, S. D. Dutta, T. V. Patil, K.-T. Lim, Functionalized chitosan/spherical nanocellulose-based hydrogel with superior antibacterial efficiency for wound healing, *Carbohydr. Polym.*, 2022, 284, 119202.
- [33] K. Wang, J. Wang, L. Li, L. Xu, N. Feng, Y. Wang, X. Fei, J. Tian, Y. Li, Synthesis of a novel anti-freezing, non-drying antibacterial hydrogel dressing by one-pot method, *Chem. Eng. J.*, 2019, 372, 216-225.
- [34] Y. Zong, B. Zong, R. Zha, Y. Zhang, X. Li, Y. Wang, H. Fang, W.-L. Wong, C. Li, An antibacterial and anti-oxidative hydrogel dressing for promoting diabetic wound healing and real-time monitoring wound pH conditions with a NIR fluorescent imaging system, *Adv. Healthc. Mater.*, 2023, 2300431.
- [35] Q. Zhang, M. Zhang, T. Wang, X. Chen, Q. Li, X. Zhao, Preparation of aloe polysaccharide/honey/PVA composite hydrogel: Antibacterial activity and promoting wound healing, *Int. J. Biol. Macromol.*, 2022, 211, 249-258.
- [36] M. Zhang, Q. Yang, T. Hu, L. Tang, Y. Ni, L. Chen, H. Wu, L. Huang, C. Ding, Adhesive, antibacterial, conductive, anti-UV, self-healing, and tough collagen-based hydrogels from a pyrogallol-Ag self-catalysis system, *ACS Appl. Mater. Interfaces*, 2022, 14(7), 8728-8742.
- [37] P. Zhao, Y. Feng, Y. Zhou, C. Tan, M. Liu, Gold@Halloysite nanotubes-chitin composite hydrogel with antibacterial and hemostatic activity for wound healing, *Bioact. Mater.*, 2023, 20, 355-367.
- [38] S. Zheng, H. Wang, P. Das, Y. Zhang, Y. Cao, J. Ma, S. Liu, Z.-S. Wu, Multitasking MXene inks

enable high-performance printable microelectrochemical energy storage devices for all-flexible self-powered integrated systems. *Adv. Mater.*, 2021, 33(10), 2005449.

[39] G. Bovone, O. Y. Dudaryeva, B. Marco-Dufort, M. W. Tibbitt, Engineering hydrogel adhesion for biomedical applications via chemical design of the junction, *ACS Biomater. Sci. Eng.*, 2021, 7, 4048-4076.

[40] X. Pei, H. Zhang, Y. Zhou, L. Zhou, J. Fu, Stretchable, self-healing and tissue-adhesive zwitterionic hydrogels as strain sensors for wireless monitoring of organ motions, *Mater. Horiz.*, 2020, 7, 1872-1882.

[41] L. Han, K. Liu, M. Wang, K. Wang, L. Fang, H. Chen, J. Zhou, X. Lu, Mussel-inspired adhesive and conductive hydrogel with long-lasting moisture and extreme temperature tolerance, *Adv. Funct. Mater.*, 2018, 28(3), 1704195.

[42] H. Zhang, X. Sun, J. Wang, Y. Zhang, M. Dong, T. Bu, L. Li, Y. Liu, L. Wang, Multifunctional injectable hydrogel dressings for effectively accelerating wound healing: enhancing biomineralization strategy, *Adv. Funct. Mater.*, 2021, 31(23), 2100093.

[43] Y. Huang, F. Shi, L. Wang, Y. Yang, B. M. Khan, K. L. Cheong, Y. Liu, Preparation and evaluation of *Bletilla striata* polysaccharide/carboxymethyl chitosan/Carbomer 940 hydrogel for wound healing, *Int. J. Biol. Macromol.*, 2019, 132, 729-737.

[44] M. Li, Z. Zhang, Y. Liang, J. He, B. Guo, Multifunctional tissue-adhesive cryogel wound dressing for rapid nonpressing surface hemorrhage and wound repair, *ACS Appl. Mater. Interfaces*, 2020, 12(32), 35856-35872.

[45] J. Hwang, Y. Cha, L. Ramos, T. Zhu, L. B. Kurnaz, C. Tang, Tough antibacterial metallopolymer double-network hydrogels via dual polymerization, *Chem. Mater.*, 2022, 34(12), 5663-5672.

[46] D. Liu, J. Qiu, R. Xu, J. Liu, J. Feng, L. Ouyang, S. Qian, Y. Qiao, X. Liu, β -CD/PEI/PVA composite hydrogels with superior self-healing ability and antibacterial activity for wound healing, *Compos. B: Eng.*, 2022, 238, 109921.

[47] J. Lu, Y. Chen, M. Ding, X. Fan, J. Hu, Y. Chen, J. Li, Z. Li, W. Liu, A 4arm-PEG macromolecule crosslinked chitosan hydrogels as antibacterial wound dressing, *Carbohydr. Polym.*, 2022, 277, 118871.

[48] H. Liu, Y. Feng, X. Cao, B. Luo, M. Liu, Chitin nanocrystals as an eco-friendly and strong anisotropic adhesive, *ACS Appl. Mater. Interfaces*, 2021, 13, 11356-11368.

[49] F. Chen, J. Qin, P. Wu, W. Gao, G. Sun, Glucose-responsive antioxidant hydrogel accelerates diabetic wound healing, *Adv. Healthc. Mater.*, 2023, 2300074. DOI:10.1002/adhm.202300074.

- [50] J. Tan, D. Wang, H. Cao, Y. Qiao, H. Zhu, X. Liu, Effect of local alkaline microenvironment on the behaviors of bacteria and osteogenic cells, *ACS Appl. Mater. Interfaces*, 2018, 10(49), 42018-42029.
- [51] C. R. Kruse, M. Singh, S. Targosinski, I. Sinha, J. A. Sørensen, E. Eriksson, K. Nuutila, The effect of pH on cell viability, cell migration, cell proliferation, wound closure, and wound reepithelialization: *in vitro* and *in vivo* study, *Wound Repair and Regeneration*, 2017, 25(2), 260-269.